Smart Agricultural Technology 1 (2021) 100024

Contents lists available at ScienceDirect

Smart Agricultural Technology

journal homepage: www.elsevier.com/locate/atech

A robust machine vision system for body measurements of beef calves

David Weales, Medhat Moussa*, Cole Tarry

School of Engineering, University of Guelph, Guelph, ON N1G 2W1, Canada

ARTICLE INFO

Keywords:
Livestock
Beef cattle
RGB-D Camera
Image processing
3D Vision

ABSTRACT

Measuring body dimensions is a useful method of assessing the health and growth of young beef cattle. However, performing these measurements in a barn environment can present a number of unique challenges. The objective of this paper is to design an image capture system and image processing algorithm that can meet these challenges. The system uses two RGB-D cameras to collect images from the top-left and top-right of the calf. Images were collected in a barn environment along with ground truth body measurements. Colour image processing was used to remove the background by making use of a deep learning instance segmentation model for each camera. The segmented data from the two cameras was registered to create a 3D image of the calf, which was then used to measure a few key body dimensions. The experimental results showed a mean error of 0.2 cm for heart girth, -0.8 cm for withers height, -0.2 cm for midpiece height, and -2.1 cm for pin height.

1. Introduction

Monitoring body conditions of livestock is an important method of assessing their growth, feeding needs, and overall health. Monitoring can be performed by taking body measurements, such as girth, length, and height at specific body locations, by assessing body weight, or through body condition scoring. These processes can be difficult to perform regularly as they may be time consuming, difficult to perform in a barn environment, and stressful for the animals involved. These processes may also require specialized equipment, such as livestock scales, or specialized training to ensure that the measurements are collected properly at the correct location. As such, many methods have been proposed for various body measurements. A recent literature review on this topic found that the most common measurements taken were a top view of the body area, withers height, hip height, body length, hip-width, body volume, and chest girth [2].

Developing a computer vision system for measuring livestock in a real barn environment presents several challenges. One of the primary challenges is the placement of optical sensors in a barn environment where space may be limited. Ideally, cameras would be placed where there is no background or foreground clutter, and where only one animal is visible in the camera frame. If depth cameras are used, then the distance to the animal should be optimized to ensure the best accuracy. To overcome this challenge, researchers have suggested installing depth cameras in areas where a single animal will pass, such as by automated feeders [9,12] or in a passageway that animals walk through [8]. In situations with a static background, background subtraction can be used [8,10]. Foreground clutter is more difficult to manage as it results in missing data whenever an object is blocking the animal. Several studies have successfully removed various types of obstacles from the foreground, resulting in partial data from the animal which could then be utilized [1,12].

Another challenge is to ensure that one animal is being measured when multiple animals are in the field of view of the camera. Most previous studies had a single animal in each image, although [5] were able to use ellipse estimation on animals in group pens to segment individual animals. Multiple cameras have also been used to collect images of an animal in motion, requiring precise synchronization of the cameras [8].

Animal posture can pose additional challenges when measuring livestock. When measuring features such as height or length, the measurements may be inaccurate if an animal is bending or twisting its body. [4] used machine learning to describe postures with curvature and deviation features for estimating body weight. Other studies have addressed the posture by analysing the curvature of the spine and discarding the samples in which the spine was not straight [3].

This paper presents a robust system for measuring young beef calves. This system was able to address the major challenges of a barn environment. Only two assumptions were made: the animals were not under direct sunlight (i.e. they are housed indoors) and there was no foreground clutter in the camera frame. The proposed system was designed and tested to overcome the following challenges arising from deployment in a real-world barn:

- The environment or infrastructure is unknown (i.e., the system should be adaptable to a wide variety of barn environments)
- The image background is not static and may include other calves that are not being measured.

* Corresponding author.
E-mail address: mmoussa@uoguelph.ca (M. Moussa).

https://doi.org/10.1016/j.atech.2021.100024
Received 12 August 2021; Received in revised form 10 November 2021; Accepted 11 November 2021

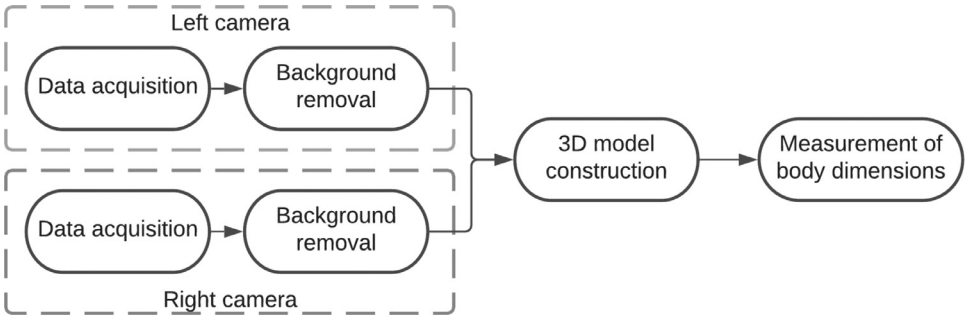

Fig. 1. Block diagram of the steps in the beef calf measurement system.

- The image may contain part of a calf or no calf at all.
- The posture of the calf is not assumed to be straight and upright (i.e., it may be bending its knees or torso).
- The calf can be in motion as the images are collected.

2. Materials and methods

2.1. Overview of the proposed system

Fig. 1 shows a block diagram of the four major steps in the system:

1. Data acquisition: An image capture system collects RGB-D images of the calves from multiple views and processes them.
2. Background removal: The RGB images are used to recognize and segment the individual calves. The background is removed and a mask containing the location of the calf is produced.
3. 3D model construction: An image processing algorithm uses the segmented mask of the calf and an aligned depth image from each camera to generate a partial 3D model of the calf.
4. Measurement of body dimensions: A 3D processing algorithm identifies physiological markers on the calf and measures relevant dimensions.

2.2. Description of image capture system and data acquisition

2.2.1. Image capture system

The system used two Intel®RealSense™ D435 cameras to capture RGB-D data. The RGB-D cameras were mounted on either side of a wooden frame 750 mm apart and 1400 mm from the ground as illustrated in Fig. 2. The cameras were angled toward one another at 22.5^{circ} from vertical in order to capture a partial view of the sides of the calf. A small touchscreen monitor was mounted on the side of the frame to provide a live camera feed and allow user input. An Intel®NUC computer was also mounted on the frame for interfacing with the cameras, accepting user input from the monitor, and storing the image data.

Fig. 3 shows the system as it is mounted in the field. As the calves moved under the system, the cameras captured images continuously.

2.2.2. Data acquisition procedure

The data collection for the beef calves took place at the Elora Beef Research Station. Data was collected over 35 days between March 24, 2020 and June 6, 2020. In total, 115 beef calves between approximately two weeks of age and eight weeks of age were imaged once a week for seven consecutive weeks.

In addition to this collection of images, contact measurements of the same calves were also collected by Vanessa Rotondo([7]). In total, 770 sets of contact measurements were collected. Each set includes the following body measurements:

- Wither height: distance from the top of the spine at the withers to the ground.
- Midpiece height: distance from the top of the spine opposite the navel to the ground.

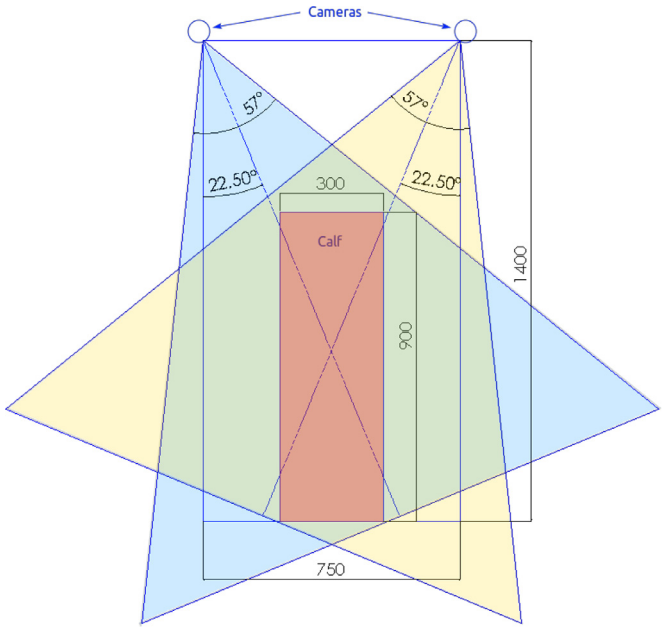

Fig. 2. Schematic diagram of the camera setup used for data collection. The field of view of the left and right cameras are shown in blue and yellow respectively. (For interpretation of the references to colour in this figure legend, the reader is referred to the web version of this article.)

- Pin height: distance from the top of the pin bone to the ground.
- Heart girth: circumference of the chest immediately behind the front legs.

These measurements were collected while the calves were standing upright with their legs straight. Once the contact measurements were completed, the calves were guided using a halter beneath the RGB-D image capture system. Efforts were made to position the calf so that it was centered in the image capture system and its posture was similar to that in the contact measurement procedure. Images were automatically collected by the image capture system once a calf was visible in the RGB-D camera. The unique identification number of each calf was recorded using the system interface. The calf was moved after 10–15 images were collected at a rate of 1 fps.

After the initial collection of the data, additional data was gathered by applying stickers to the body of each calf. The locations of these stickers are shown in Fig. 4. This allowed a precise comparison between the contact and non-contact measurements at the same location. Of the 115 beef calves that were measured in the field, three had physical green markers placed at the contact measurement locations.

Fig. 3. RGB-D image capture system collecting images of a calf.

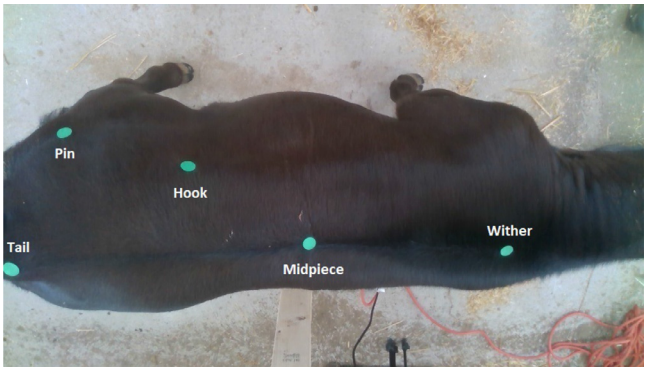

Fig. 4. Green stickers used to mark measurement locations on the calf.

2.3. Background removal

The imaging system was designed to trigger the image capture process automatically whenever an object was in the center of the FOV of the camera. This reflected the importance of capturing images of moving animals while placing few restrictions on the movement of other animals or workers. This mimicked how the system could be used in a real-world environment. Yet this also created several problems. Multiple animals might appear in the same image. Some or all of the animals might have part of their body captured in the same image. As such, it was necessary to pre-process each image to remove the background and segment instances of animals whose full body was captured in one image. This simplified the 3D construction of the body that is described in the following section.

Instance segmentation of the calves from the background data was performed using the Detectron2 deep learning framework [11]. The Model Zoo used a Mask R-CNN with a ResNet50 + FPN backbone trained with 3x schedule. Instead of using the images of the beef calves, images captured by the same system from a dairy calf facility were used as the backgrounds of the latter set were more cluttered than the beef dataset. This allows the model to be more robust to background clutter. In total, 104 images of five different dairy calves were collected and labelled. The

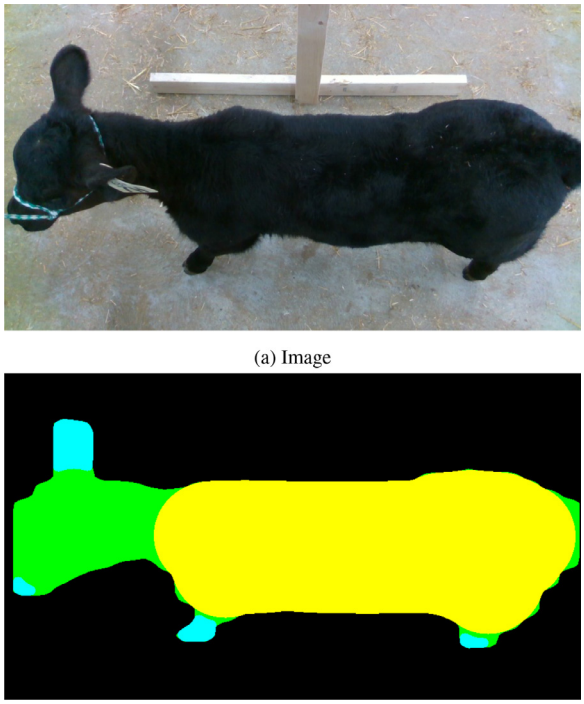

(a) Image

(b) Segmented mask

Fig. 5. Morphology applied to the mask of the calf to separate the smaller sections of the calf (shown in green and blue) from the main body (shown in yellow). (For interpretation of the references to colour in this figure legend, the reader is referred to the web version of this article.)

labels were made by drawing a polygon around every calf in the image. The dataset was randomly separated into a 80-10-10% train-validate-test split and trained for 1000 iterations. To evaluate the test set, the average precision was taken using IoU thresholds from 0.5 to 0.95 with a step size of 0.05, which is the primary challenge metric for the COCO dataset [6]. The detection was considered valid if the confidence was at least 50%. Using these metrics, the segmentation reached an overall average precision of 86% on the test set.

The segmentation stage was able to segment a calf from the background, but it did not identify whether the segmentation contained the entire body of the calf or a partial section. As such, the next step was to identify if the full body of the calf was visible in the RGB images from both cameras. In order to determine if the full body of the calf was visible, it was necessary to identify if all four legs were visible in the RGB images. Since there is one camera on either side of the calf, two legs should be visible in the left camera and two legs should be visible in the right camera. The legs are detected by analysing the shape of the mask provided by the instance of the segmentation stage. Using a morphological open operation on the mask, the smallest sections, such as the ears and legs of the calf, were removed from the mask. Using another morphological open operation with a larger kernel allowed a rough separation of the body from the neck of the calf. The impact of these operations is shown in Fig. 5.

Once the body was roughly separated from the head and legs, additional operations were performed to check if the entire body of the calf was visible in the image. Since the body measurements were not concerned with the head or neck, a calf was assumed to be fully visible if two legs could be detected in the images from each camera. The legs were identified by examining the segmented mask and determining the number of individual contours above or below the body contour in the image. To do so, the centroid of each contour was identified. If the centroids of two smaller contours were both higher or both lower than the body contour, it was assumed that both legs were visible in the image.

(a) RGB image

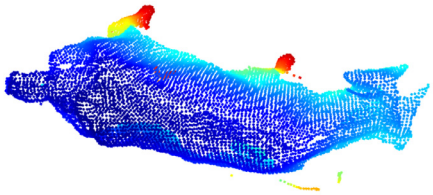

(b) Point cloud

Fig. 6. Example of RGB segmentation applied to the 3D point cloud from the Realsense camera.

2.4. 3D Model construction

The RealSense cameras provided depth images that were aligned with the RGB, and as such the predicted mask from the instance segmentation could be applied directly to the depth image from each camera. If multiple masks were available, the one that was most visible (i.e., contained the most pixels) was assumed to be the calf being measured. The depth data from each camera was also converted with the help of the camera intrinsics into a 3D point cloud. An example of the 3D segmentation and point cloud development is shown in Fig. 6.

Next, the 3D data from the two cameras was combined into a single 3D point cloud using the transformation matrix between the cameras. This matrix was calculated given that the cameras were in a fixed orientation relative to each other. Then the entire 3D point cloud was transformed so its coordinate frame z-axis orientation was normal to the ground and the origin $z = 0$ was placed at the ground level.

Once the 3D model was constructed and aligned with the ground, additional cleaning stfigure were performed. Any points less than 5 cm above the ground were removed to crop out any remaining sections of the floor that the semantic segmentation missed. The cloud was downsampled using a voxel size of 0.01 m to reduce the computation time of the later stages of the algorithm. Lastly, noise was removed using radius outlier removal. This step was performed twice, first using a radius of 0.05 m and a minimum of 25 points, then again with a radius of 0.2 m and a minimum of 250 points.

Due to the location of the image capture system in the field, the calves always approached from the same direction. However, as it was possible for the calves to approach from different angles, the body had to be oriented in a consistent manner. To align the spine of the calf with the y-axis, an ellipse was fit to the xy plane as shown in Fig. 7. A rotation transform was then implemented around the z-axis so that the major axis of the ellipse was aligned with the y-axis of the world frame.

In some cases, the body of the calf could be twisted so that its spine was not straight. This scenario was identified by comparing the angle of the front half of the body with the angle of the rear half. If the difference between the angles was greater than 15^{circ}, the image was discarded due to the difficulty involved in measuring a calf in a twisted position.

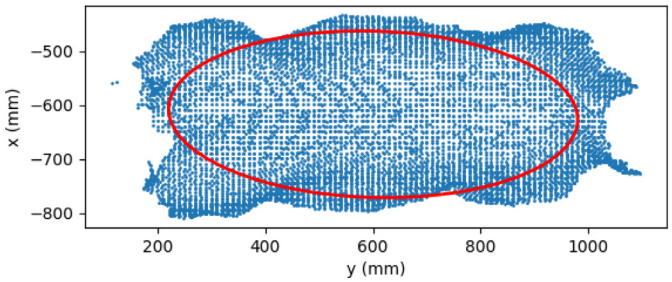

Fig. 7. Fitting an ellipse to the xy data to determine the angle of the calf body.

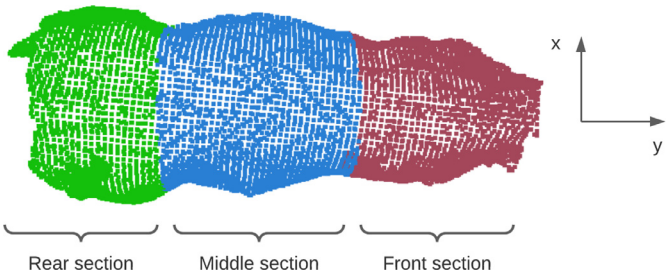

Fig. 8. Top view of the body point cloud separated into 3 equal sections.

2.5. Measurement of body dimensions

Using the segmented 3D model of the calf, the following body measurements were computed and compared with the ground truth:

Height measurements

- Withers: located at the shoulders of the calf above the front legs.
- Midpiece: located at the stomach of the calf above the navel.
- Pins: located at the top of the pin bones of the rear legs.

Girth measurements

- Heart: located at the stomach of the calf just behind the front legs.

The process of computing these measurements started by separating the body of the calf into three equal sections along the direction of the spine. The x-axis and y-axis were defined along and perpendicular to the direction of the spine as shown in 8. The front, middle, and rear sections contained the withers, midpiece, and pins respectively.

The steps for detecting the withers, midpiece, and pin locations within the three segments are described in the following sections.

2.5.1. Location of the withers

An approximation of the location of the withers was obtained by using the widest point in the front section of the calf. The procedure for detecting the widest point is described in Algorithm 1 .

Algorithm 1: Localization of wither point on the y-axis.

```
Result: Withers location
Separate the front section of the calf into 10 subsections;
width_max ← 0 ;
foreach subsection do
    width ← max(x) − min(x);
    if width > width_max then
        width_max ← width;
        wither ← subsection;
    end
end
```

The height of the withers was measured from the highest point on the point cloud to the ground. However, the ground truth measure of

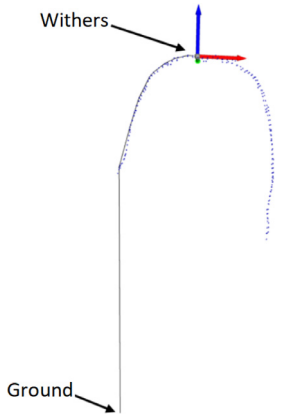

Fig. 9. Measurement of the wither height on the point cloud.

the withers included part of the body curvature since it was collected using a flexible measuring tape placed on the left side of the calf. To approximate this effect, a convex hull was created to follow the body of the calf from the highest point to the ground. A sample of the height measurement of the withers is shown in Fig. 9.

2.5.2. Location of the midpiece

An approximation of the midpiece location was obtained by using the widest point in the middle section of the calf. The procedure for detecting the widest point is described in Algorithm 2 . The midpiece height was measured using a convex hull similar to the approach used for the height of the withers.

Algorithm 2: Localization of midpiece point on the y-axis.

Result: Midpiece location
Separate the middle section of the calf into 10 subsections along the y-axis;
$width_{\max} \leftarrow 0$;
foreach *subsection* **do**
  $width \leftarrow \max(x) - \min(x)$;
  if $width > width_{\max}$ **then**
    $width_{\max} \leftarrow width$;
    $midpiece \leftarrow subsection$;
  end
end

2.5.3. Pin location

An approximation of the location of the pin was obtained by using the widest point in the rear section of the calf. The rear section of the calf has a more uniform width and therefore it is difficult to precisely locate the point with the largest width. As such, the location of the pin was approximated by finding the widest section that was closest to the rear of the calf. The procedure for detecting the widest point is described in Algorithm 3 .

While the heights of the withers and midpiece can be measured from the highest point of the spine, the top of the pin bone is located on the side of the calf. The location of the pin bone was approximated by examining a cross-section of the region of the pin (i.e., the x-z plane). The procedure for estimating the location is described in Algorithm 4 . Once the pin bone location was approximated, the pin height was measured as the distance from the top of the pin bone to the ground.

2.5.4. Heart location

The location of the heart was approximated by examining the area between the withers and the midpiece as shown in Fig. 10. The heart was identified as the area just behind the front leg where the chest became thinner. Depending on the posture of the calf, the front legs may not be aligned so each side of the calf was analyzed independently. The procedure for estimating the heart location is detailed in Algorithm 5 .A sample of the estimated heart location on each side of the body is shown in Fig. 11.

The heart girth was measured as the perimeter around the heart on the point cloud. As the cameras were mounted above the calf on either side, there was only a partial view of the top and sides of the heart girth. As such, the perimeter was calculated from the available partial data and then the value was scaled to estimate the full girth. To reduce noise from the regions farthest from the camera, the cross-section was cropped at 80% of the maximum height. Then the convex hull perimeter (P) was scaled following 1. The scale value of 1.519 was determined empirically from the measurements and was only valid using this approach. A sample heart girth measurement is shown in Fig. 12.

$$HG = 1.5191P \tag{1}$$

Algorithm 3: Localization of the pin point on the y-axis.

Result: Pin location
Separate the rear section of the calf into 10 subsections along the y-axis;
Start at the subsection closest to the front of the calf;
$width_{\max} \leftarrow (max(x) - \min(x))$;
foreach *subsection* **do**
  $width \leftarrow \max(x) - \min(x)$;
  if $width > 0.95 width_{\max}$ **then**
    $width_{\max} \leftarrow width$;
    $pin \leftarrow subsection$;
  else
    continue;
  end
end

Algorithm 4: Localization of pin bone point.

Result: Location of the top of the pin bone
Remove points $z < 0.8max(z)$;
Separate the pin section into 10 subsections along the z-axis;
Start at the subsection at the top of the calf;
$width_{\max} \leftarrow (max(x) - \min(x))$;
foreach *subsection* **do**
  $width \leftarrow \max(x) - \min(x)$;
  if $width > 0.5 width_{\max}$ **then**
    $width_{\max} \leftarrow width$;
    $pin \leftarrow subsection$;
    break;
  end
end

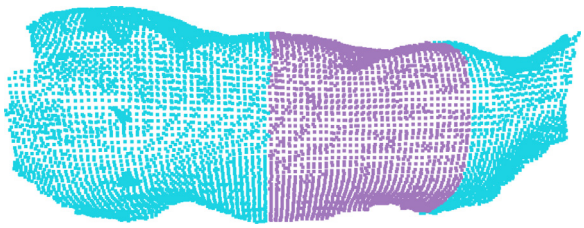

Fig. 10. Top view of the 3D image showing the region between the wither and midpiece.

Algorithm 5: Localization of the heart point on the y-axis.

Result: Heart location
$x_{mid} \leftarrow \frac{max(x)+\min(x)}{2}$;
Separate points into two sets: where $x > x_{mid}$ and where $x < x_{mid}$;
foreach *set* **do**
  Remove points at $z > 0.7max(z)$ and $z < 0.7max(z) - 2$cm;
  Separate the remaining points into 20 subsections along the y-axis;
  Start at the subsection closest to the rear of the calf;
  $width_{previous} \leftarrow 0$;
  foreach *subsection* **do**
    $width \leftarrow abs(mean(x) - x_{mid})$;
    ;
    $ratio \leftarrow \frac{width - width_{previous}}{width_{previous}}$ **if** $ratio > 2$ **then**
      heart ← subsection;
      break;
    else
      $width_{previous} \leftarrow width$;
    end
  end
end

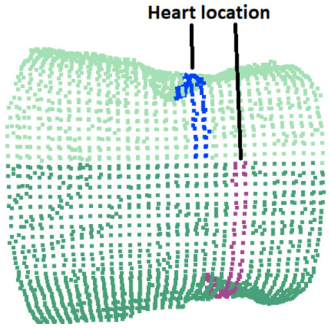

Fig. 11. Estimated location of the heart on both sides of the calf's chest.

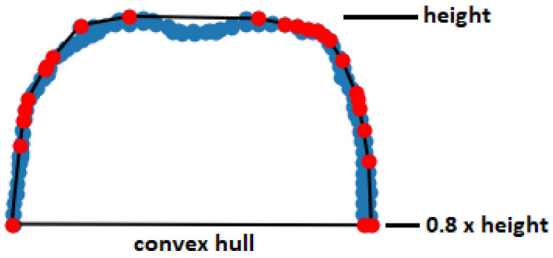

Fig. 12. Measurement of the heart girth on the point cloud.

Table 1
Mean and standard deviation of error between the height of the non-contact and contact measurements at the marker locations.

Location	Images	Mean (%)	Mean (cm)	Std dev (cm)
Wither	157	-5.1	-4.6	0.6
Midpiece	152	-3.3	-3.1	1.0
Pin	161	-4.0	-3.2	2.1

3. Results

For these calves, a total of 161 images were collected that could be used for measurement. Table 1 shows the average error between using contact and non-contact measurements when measured from the green marker locations.

Table 2
Mean and standard deviation of the difference between non-contact and contact measurements taken at the approximated locations.

Dimension	Images	Mean (%)	Mean (cm)	Std dev (cm)
Heart	7261	0.3	0.2	5.5
Wither	6841	-0.9	-0.8	4.5
Midpiece	7085	-0.2	-0.2	2.1
Pin	6709	-2.8	-2.1	4.6

For the remaining 112 calves, 679 field measurements were completed. For these calves 8635 images were extracted for non-contact measurements: a median of nine images per calf per day. To reduce the effect of outliers, the highest and lowest measurements for each calf were removed for each day. As a result, each measurement was calculated using a median of seven images. Table 2 shows the mean and standard deviation of the difference between contact and non-contact measurements.

4. Discussion

The results showed that the system performed well when compared to similar systems reported in the literature. [8] achieved an average error of 1.9% for the height of the withers and 2.3% for the heart girth, and [12] achieved an average error of 2.14% for the heart girth. The results in Table 1 and Table 2 were obtained while the calves were moving, which shows the robustness of the current system in a real-world environment.

The system had two potential sources of errors. One was related to the design of the 3D system and the resultant 3D image. The other was related to errors in estimating the non-contact measurement location. The overall accuracy of the system was impacted by both sources of errors. There could also potentially be slight error due to the small delay between capturing the images from each camera. However, the motion of the calves was slow enough that this was not expected to cause any issues.

It was noted that the mean errors reported in Table 1 were higher than the ones reported in Table 2. Since the measurements in Table 1 were collected from only three calves on a single day, it is difficult to determine the exact reason for the increased error rate in this Table. Possible reasons could include that the calves were in a poor posture for measurement, or that the method of measuring the point cloud tended to underestimate the height. As calves are taller in the rear than they are in the front, the locations of the withers and midpiece might have been approximated further to the rear of the calf. This would result in a higher measurement, which would counteract the underestimation. It was also noted that the ground truth contact measurements themselves contained errors based on slight differences in the posture of the calf, differences in how people read the measuring devices, or variations in the measurements taken from slightly different locations or angles.

5. Conclusion

This paper has presented the development of a robust automated system for measuring calves in a barn environment. This system did not require the animal to be stationary while taking non-contact measurements. Field testing and validation showed that the system is highly accurate in estimating four body measurements: the withers, mid-piece, pin, and the heart girth.

Declaration of Competing Interest

The authors declare that they have no known competing financial interests or personal relationships that could have appeared to influence the work reported in this paper.

Acknowlgedgments

We would like to acknowledge Vanessa Rotondo who provided the contact measurements data for the calves. This research is supported by funding from the Food from Thought Digital Agriculture Research Fund at the University of Guelph.

References

[1] Y. Cang, H. He, Y. Qiao, An intelligent pig weights estimate method based on deep learning in sow stall environments, IEEE Access 7 (2019) 164867–164875, doi:10.1109/ACCESS.2019.2953099.

[2] R. Dohmen, C. Catal, Q. Liu, Computer vision-based weight estimation of livestock: a systematic literature review, New Zealand Journal of Agricultural Research 0 (0) (2021) 1–21, doi:10.1080/00288233.2021.1876107.

[3] A.F.A. Fernandes, J.R.R. Dórea, R. Fitzgerald, W. Herring, G.J.M. Rosa, A novel automated system to acquire biometric and morphological measurements and predict body weight of pigs via 3D computer vision1, Journal of animal science 97 (1) (2019) 496–508, doi:10.1093/jas/sky418.

[4] K. Jun, S.J. Kim, H.W. Ji, Estimating pig weights from images without constraint on posture and illumination, Computers and Electronics in Agriculture 153 (2018) 169–176, doi:10.1016/j.compag.2018.08.006.

[5] M. Kashiha, C. Bahr, S. Ott, C.P.H. Moons, T.A. Niewold, F.O. Ödberg, D. Berckmans, Automatic weight estimation of individual pigs using image analysis, Computers and Electronics in Agriculture 107 (2014) 38–44, doi:10.1016/j.compag.2014.06.003.

[6] Lin, T.-Y., Maire, M., Belongie, S., Bourdev, L., Girshick, R., Hays, J., Perona, P., Ramanan, D., Zitnick, C. L., Dollár, P., 2015. Microsoft coco: Common objects in context. 1405.0312.

[7] Rotondo, V., 2021. Masters thesis.

[8] A. Ruchay, V. Kober, K. Dorofeev, V. Kolpakov, S. Miroshnikov, Accurate body measurement of live cattle using three depth cameras and non-rigid 3-d shape recovery, Computers and Electronics in Agriculture 179 (2020) 105821, doi:10.1016/j.compag.2020.105821.

[9] X. Song, J. Schutte, P.V.D. Tol, F.V. Halsema, P.W.G. Groot, Body measurements of dairy calf using a 3-D camera in an automatic feeding system, in: AgEng 2014: International Conference of Agricultural Engineering, 2014. Zurich, Switzerland

[10] Y. Wang, W. Yang, P. Winter, L. Walker, Walk-through weighing of pigs using machine vision and an artificial neural network, Biosystems Engineering 100 (1) (2008) 117–125, doi:10.1016/j.biosystemseng.2007.08.008.

[11] Y. Wu, A. Kirillov, F. Massa, W.-Y. Lo, R. Girshick, in: Detectron2, 2019. https://github.com/facebookresearch/detectron2

[12] X. Zhang, G. Liu, L. Jing, S. Chen, Automated measurement of heart girth for pigs using two kinect depth sensors, Sensors 20 (14) (2020) 3848, doi:10.3390/s20143848.